Dynamics of the Gay-Berne fluid

Enrique de Miguel* and Luis F. Rull
Departamento de Física Atómica, Molecular y Nuclear, Universidad de Sevilla, Apartado 1065, Sevilla 41080, Spain

Keith E. Gubbins
School of Chemical Engineering, Cornell University, Ithaca, New York 14853
(Received 25 June 1991)

Using molecular-dynamics computer simulation, we study the dynamical behavior of the isotropic and nematic phases of highly anisotropic molecular fluids. The interactions are modeled by means of the Gay-Berne potential with anisotropy parameters $\kappa=3$ and $\kappa'=5$. The linear-velocity autocorrelation function shows no evidence of a negative region in the isotropic phase, even at the higher densities considered. The self-diffusion coefficient parallel to the molecular axis shows an anomalous increase with density as the system enters the nematic region. This enhancement in parallel diffusion is also observed in the isotropic side of the transition as a precursor effect. The molecular reorientation is discussed in the light of different theoretical models. The Debye diffusion model appears to explain the reorientational mechanism in the nematic phase. None of the models gives a satisfactory account of the reorientation process in the isotropic phase.

PACS number(s): 61.20.Ja, 61.30.By, 64.70.Md

I. INTRODUCTION

The formalism of time-dependent correlation functions is a powerful tool in understanding the dynamical processes involved in molecular fluids [1, 2]. It provides a suitable framework in which a wide variety of experiments can be interpreted. However, this is a far from trivial task. Many observations tend to be influenced by more than one dynamical process (collision-induced effects, vibrational relaxation, etc.) and they cannot be easily identified by experimental considerations alone [3]. In this sense, computer simulation is of great value because it can discern the various processes. Furthermore, it is possible to evaluate certain correlation functions in the course of a simulation which are not easily obtained from experiments.

There is also great interest in understanding the physical nature of molecular motion in liquids. Computer simulations using molecular-dynamics methods have been mainly focused on the applicability of theoretical models of molecular reorientation, such as the diffusion models of Gordon [4], and the stochastic Langevin model [5]. Attention has also been given to predicting correlation functions from memory functions approximations [1,6–8] and truncated cumulant expansions [9, 10].

The computer simulation of the dynamical behavior of molecular fluids has proceeded along two fronts: (a) simulation of real fluids using suitable model potentials [1, 11–20] and (b) simulations of highly idealized models of molecular fluids. The latter is the approach followed in the study of the dynamics of hard-body molecules, such as spherocylinders [21], prolate and oblate ellipsoids of revolution [22–24] infinitely thin hard rods [25, 26], etc.

In this paper we follow the second approach, reporting the results of a molecular-dynamics study of the translational and rotational motion in the Gay-Berne (GB) model fluid [27] with anisotropy parameters $\kappa=3$ and $\kappa'=5$. Here κ is the ratio between the long and minor axis of the ellipsoidal molecule and κ' is the well-depth ratio for the side-by-side and end-to-end configurations. Two reasons lead us to undertake such an study. First, it would be desirable to know to what extent the dynamical processes in highly anisotropic systems differ from those in fluids of small linear molecules. To our knowledge, only limited studies have been reported for highly elongated molecules [21–26, 28–30]. Second, it would be of great interest to know how the onset of orientational order influences the dynamical behavior of the fluid. The GB fluid has been shown to form mesogenic phases at high densities [31–36]. In a previous publication [36], we have shown that a stable nematic phase is formed at temperatures above $T^*\approx0.80$ and, at sufficiently high densities, a Sm-B phase. Below $T^*\approx0.80$, the orientationally disordered isotropic phase directly transforms into the Sm-B phase [33].

In the present paper we focus on the single-particle translational and rotational dynamics emphasizing the diffusion process and the reorientational dynamics. We limit our study to the translationally disordered phases (isotropic and nematic). In particular, we consider the dynamics of the isotropic phase for six state points at different reduced temperatures and densities: (1) $T^*=0.90$, $\rho^*=0.130$; (2) $T^*=0.80$, $\rho^*=0.150$; (3) $T^*=0.70$, $\rho^*=0.170$; (4) $T^*=0.60$, $\rho^*=0.190$; (5) $T^*=0.50$, $\rho^*=0.210$; (6) $T^*=0.45$, $\rho^*=0.230$. The liquid-vapor critical point for the GB fluid is located [35] at $T_c^*\approx0.49$ and $\rho_c^*\approx0.095$ and the temperature of the triple point is $T_t^*\approx0.38$. Hence this choice corresponds to state points well above the critical point up to temper-

atures and densities close to the triple point along the liquid side of the vapor-liquid coexistence curve. In addition, we study the temperature dependence of the self-diffusion coefficient in the isotropic phase. This was accomplished along the isochore $\rho^*=0.230$, with temperatures varying from $T^*=0.45$ up to $T^*=2.00$. The dynamical behavior of the nematic fluid is studied at $T^*=0.95$. According to previous work [36], the GB fluid undergoes a weakly-first-order isotropic-nematic transition at this temperature for densities $\rho_I^*=0.308$ and $\rho_N^*=0.314$.

In Sec. II we include a brief summary of the computational methodology. In Sec. III we describe the translational motion of the Gay-Berne fluid. In Sec. IV we study the orientational dynamics of this fluid and the results are analyzed in terms of different models for molecular reorientation.

II. COMPUTER-SIMULATION DETAILS

The explicit expression of the potential between a pair of molecules in the Gay-Berne model [27] is given by

$$U_{\rm GB}=4\epsilon(\hat{\mathbf{r}},\hat{\mathbf{u}}_1,\hat{\mathbf{u}}_2)\left[\left[\frac{\sigma_0}{r-\sigma(\hat{\mathbf{r}},\hat{\mathbf{u}}_1,\hat{\mathbf{u}}_2)+\sigma_0}\right]^{12}-\left[\frac{\sigma_0}{r-\sigma(\hat{\mathbf{r}},\hat{\mathbf{u}}_1,\hat{\mathbf{u}}_2)+\sigma_0}\right]^{6}\right], \tag{1}$$

where $\hat{\mathbf{u}}_i$ is the axial vector of molecule i and $\hat{\mathbf{r}}$ is the vector along the intermolecular vector $\mathbf{r}$; $\sigma(\hat{\mathbf{r}},\hat{\mathbf{u}}_1,\hat{\mathbf{u}}_2)$ and $\epsilon(\hat{\mathbf{r}},\hat{\mathbf{u}}_1,\hat{\mathbf{u}}_2)$ are the orientation-dependent range and strength parameters, respectively, defined in Ref. [27]. These quantities depend on the parameters κ (molecular elongation) and κ' (ratio of the potential-well depths for the side-by-side and end-to-end configurations).

The dynamical behavior of the GB fluid has been analyzed in terms of time autocorrelation functions (ACF's) defined by

$$\phi_A(t)=\frac{\langle \mathbf{A}(t_0)\cdot\mathbf{A}(t_0+t)\rangle}{\langle \mathbf{A}(t_0)\cdot\mathbf{A}(t_0)\rangle}, \tag{2}$$

where $\mathbf{A}(t)$ is a classical dynamical property of molecule i evaluated at time t. In our case, we have calculated $\phi_A(t)$ for $\mathbf{A}$ being the linear velocity of the center of mass ($\mathbf{v}$), the force ($\mathbf{F}$), the angular velocity (ω), and the torque (Γ). In addition, we have also evaluated the ACF's $\phi_{v_\parallel}(t)$, $\phi_{v_\perp}(t)$, $\phi_{F_\parallel}(t)$, and $\phi_{F_\perp}(t)$, where the subscripts $\parallel$ and $\perp$ refer to the component of the corresponding property parallel and perpendicular to the initial direction of the molecular axial vector, respectively.

To study the reorientational motion, we have calculated the self-particle reorientational correlation functions defined by

$$\phi_l(t)=\langle P_l(\hat{\mathbf{u}}(t_0)\cdot\hat{\mathbf{u}}(t_0+t))\rangle, \tag{3}$$

for $l=1$ and 2, where $\hat{\mathbf{u}}(t)$ is a unit vector along the symmetry axis of molecule i and P_l is the lth-order Legendre polynomial. In the above expressions, the angular brackets imply an average over particles as well as over time origins. According to these definitions, the correlation functions are normalized to unity. For the evaluation of the ACF's, the spacing between consecutive time origins was $t_0^*=10\Delta t^*$ where $\Delta t^*=0.0015$ is the time step, in reduced units $[\Delta t^*=(m\sigma_0^2/\epsilon_0)^{-1/2}\Delta t]$, used in the integration of the equations of motion. The long tail of the ACF's was calculated up to a time span of 800–1000 t_0^*. The correlation time associated with a given correlation function is defined by

$$\tau_A=\int_0^\infty dt\,\phi_A(t). \tag{4}$$

The molecular-dynamics program was the same as that used in earlier works [33, 34]. The calculations were all made for 256 molecules interacting through the GB potential. The molecules were given a moment of inertia $I^*=1$. Reduced units are used for all the quantities including temperature $T^*=k_BT/\epsilon_0$, density $\rho^*=\rho\sigma_0^3$; time $\tau^*=\tau(m\sigma_0^2/\epsilon_0)^{-1/2}$, moment of inertia $I^*=I(m/\sigma_0^2)^{-1}$, and diffusion coefficient $D^*=D(m\epsilon_0/\sigma_0^2)^{-1/2}$. The trajectories of the particles were followed for a total of 10 000 time steps after an initial equilibration period of 4000–6000 steps.

III. TRANSLATIONAL DYNAMICS

A. Translational motion

The motion of the center of mass has been analyzed in terms of the velocity ACF (VACF) and the force ACF (FACF), defined by

$$\phi_v(t)=\frac{\langle \mathbf{v}(t_0)\cdot\mathbf{v}(t_0+t)\rangle}{\langle \mathbf{v}(t_0)\cdot\mathbf{v}(t_0)\rangle}, \tag{5a}$$

$$\phi_F(t)=\frac{\langle \mathbf{F}(t_0)\cdot\mathbf{F}(t_0+t)\rangle}{\langle \mathbf{F}(T_0)\cdot\mathbf{F}(t_0)\rangle}, \tag{5b}$$

where $\mathbf{v}$ is the velocity of the center of mass of a molecule and $\mathbf{F}$ is the total force acting on each individual molecule.

In Fig. 1 $\phi_v(t)$ is illustrated for the isotropic phase. For all the state points considered, $\phi_v(t)$ shows an initial rapid Gaussian-like decay; afterwards, the collisions randomize the velocity and $\phi_v(t)$ decays smoothly. As the temperature is lowered or the density increased, the relaxation process is faster due to an increase of the collision rate with neighboring particles. There are two striking features in the VACF's shown in Fig. 1. First, there is no evidence of a negative lobe even for the highest density, close to the triple point. This is in marked contrast to the usual behavior exhibited by other dense molecular fluids, where the VACF decays to a negative value and, with a few damped oscillations, goes to zero while remaining negative [1, 11–17]. Second, as the density is increased, the system seems to develop an intermediate regime between the initial Gaussian region and the subsequent monotonic decay. This regime results in a small positive plateau in the VACF before the system enters the quasiexponential decay region.

The nature of this positive plateau becomes clearer in Fig. 2, where the VACF is shown at $T^*=0.95$ below and above the isotropic-nematic transition ($\rho_I^*=0.308$,

$\rho_N^*=0.314$). At a density 0.280, the intermediate plateau is evident. As the density is increased, the flat region eventually develops a positive minimum and maximum after which the smooth-decay regime follows. When the system is well inside the nematic phase, this structure in the VACF is even clearer. This behavior can be understood by monitoring the time relaxation of the parallel and perpendicular components of the velocity along the molecular axis at time $t=0$. This is shown in Fig. 2, where the VACF's $\phi_{v_\parallel}(t)$ and $\phi_{v_\perp}(t)$ are represented along with $\phi_v(t)$. From this figure it is apparent that the structure of the VACF is due to the behavior of the perpendicular component of the velocity. When nematic ordering has taken place in the system, $\phi_{v_\perp}(t)$ reaches a negative minimum and a positive maximum at the same time values as those in $\phi_v(t)$. On the other hand, $\phi_{v_{\parallel}(t)}$ relaxes more slowly and eventually develops a negative lobe at sufficiently long times for the higher nematic densities. The behavior of $\phi_v(t)$ seems to indicate that in the orientationally ordered phase the translational motion can be understood as if the individual molecules were diffusing along cylindrical cages. The reversal in the perpendicular component and its oscillatory character can then be ascribed to periodic rebounds with this local structure, while the parallel component undergoes a diffusive motion along the cylindrical cage.

It is interesting to note that just below the isotropic-nematic transition, this local structure starts to manifest itself. This pretransitional effect, which results in $\phi_{v_\parallel}(t)>\phi_{v_\perp}(t)$, will be discussed in Sec. III B.

The FACF in the isotropic phase is shown in Fig. 3. These functions exhibit the same qualitative features as those found for other molecular fluids [11–13, 15]. A deep negative minimum is reached after a rapid initial decay and afterwards, the functions show oscillatory behavior about zero. The only effect of varying the temperature or the density is that the FACF develops a distinct positive maximum for the lower temperatures or higher densities.

The correlation times were obtained by numerical integration of the corresponding ACF up to an upper limit $t^*_{\max}=150t_0^*$ for τ_F and $t^*_{\max}=300t_0^*$ for τ_v. From the definition of ϕ_F, the correlation time τ_F should be zero. For all the state points, we found $\tau_F^*<3\times10^{-4}$, which is zero within the accuracy of the simulations. Following

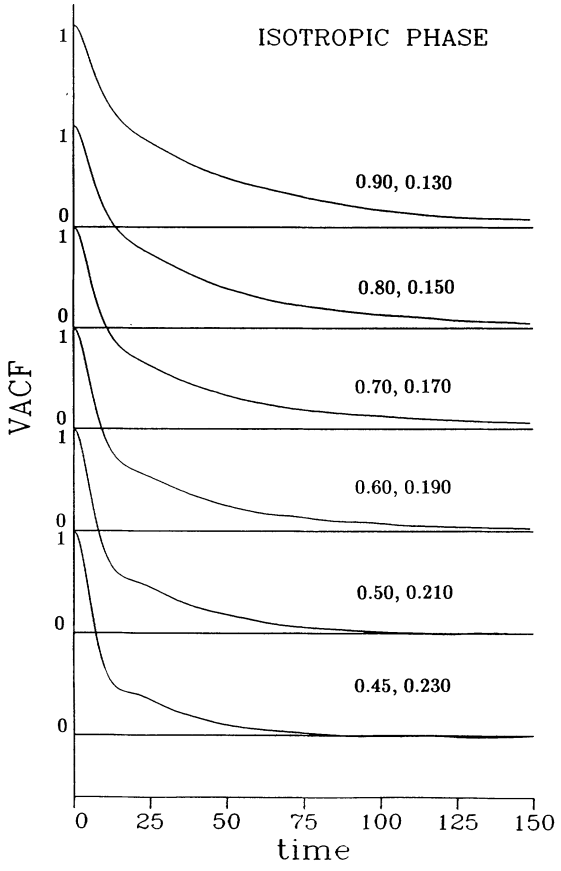

FIG. 1. Velocity autocorrelation function in the isotropic phase. The curves have been labeled according to the reduced temperature ($T^*=k_BT/\epsilon_0$) and the density ($\rho^*=\rho\sigma_0^3$); thus 0.90, 0.130 means $T^*=0.90$, $\rho^*=0.130$. The time has been expressed in units of t_0^*, where $t_0^*=10\Delta t^*=0.015(m\sigma_0^2/\epsilon_0)^{-1/2}$.

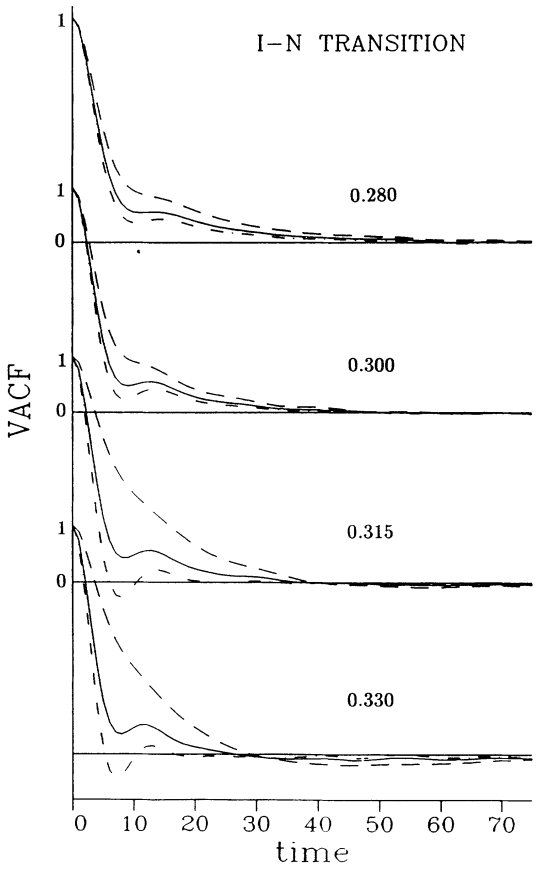

FIG. 2. Velocity autocorrelation function (full line) in the isotropic-nematic region at $T^*=0.95$. The curves have been labeled indicating the density in reduced units ($\rho^*=\rho\sigma_0^3$). Dashed line, velocity autocorrelation function parallel to molecular axis [$\phi_{v_\parallel}(t)$]; dash-dotted line, velocity autocorrelation function perpendicular to molecular axis [$\phi_{v_\perp}(t)$].

TABLE I. Self-diffusion coefficients for the GB fluid obtained from Eq. (6) (D^*) and Eq. (7) (D_E^*). The parallel and perpendicular coefficients are obtained by integrating the corresponding velocity autocorrelation function. The results for $T^*=0.95$ are for the isotropic-nematic region. The rest are for the isotropic phase.

T^*	ρ^*	D^*	D_E^*	$D_\parallel^*$	$D_\perp^*$	$D_\parallel^*/D_\perp^*$
			Isotropic phase			
0.45	0.230	0.096	0.097	0.105	0.092	1.15
0.50	0.210	0.128	0.129	0.128	0.128	1.00
0.60	0.190	0.209	0.199	0.254	0.186	1.36
0.70	0.170	0.296	0.296	0.324	0.281	1.15
0.80	0.150	0.366	0.349	0.382	0.357	1.07
0.90	0.130	0.489	0.465	0.490	0.486	1.01
			Isotropic nematic region			
0.95	0.270	0.115		0.140	0.102	1.37
0.95	0.280	0.103		0.132	0.086	1.52
0.95	0.290	0.098		0.125	0.084	1.49
0.95	0.295	0.086		0.114	0.072	1.58
0.95	0.300	0.078		0.101	0.066	1.54
0.95	0.305	0.065		0.096	0.049	1.97
0.95	0.310	0.067		0.117	0.042	2.80
0.95	0.315	0.067		0.122	0.040	3.04
0.95	0.320	0.060		0.113	0.034	3.32
0.95	0.325	0.056		0.110	0.030	3.67
0.95	0.330	0.046		0.097	0.023	4.22
0.95	0.335	0.048		0.092	0.021	4.38
0.95	0.340	0.042		0.087	0.019	4.58

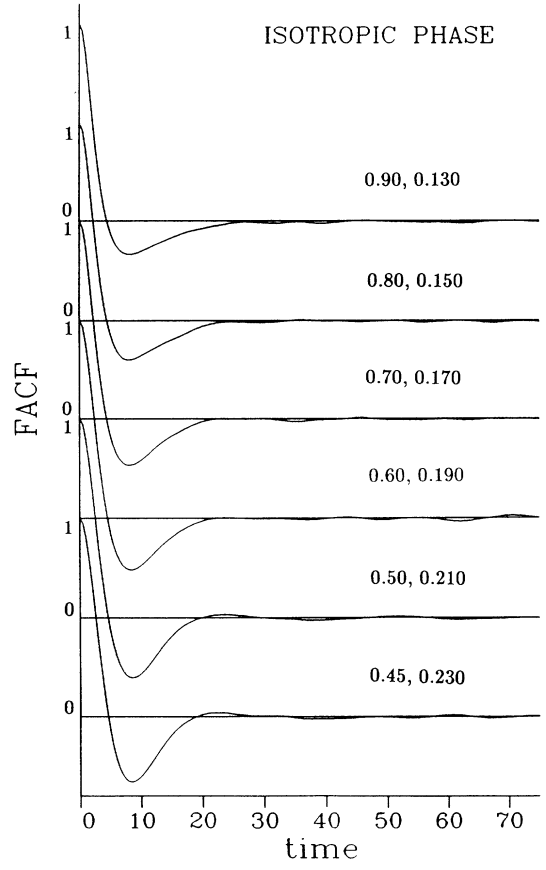

FIG. 3. Force autocorrelation function in the isotropic phase. The curves have been labeled according to the temperature and density in reduced units.

the prescriptions of Zwanzig and Ailawadi [37] for estimating the errors in the ACF's, we believe that the correlation-time values are affected by a margin of error of $\approx 5\%$. The τ_v values were used to calculate the self-diffusion coefficients (see following section).

B. Self-diffusion

From the velocity correlation time, the self-diffusion coefficient D can be obtained using the relation

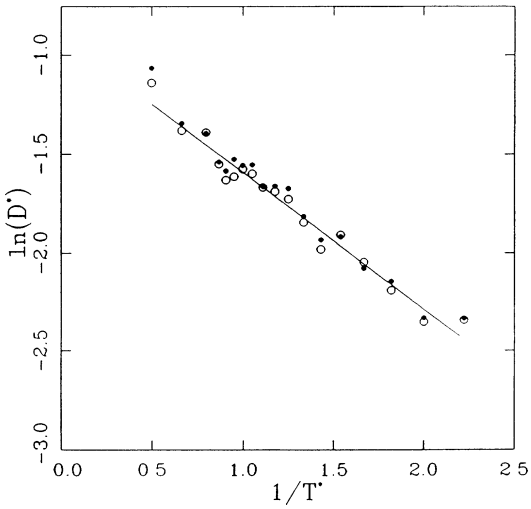

FIG. 4. Temperature dependence of the self-diffusion coefficient in the isotropic phase along the isochore $\rho^*=0.230$; open circles are for the diffusion constant as obtained from the velocity correlation time [Eq. (6)]; solid circles are for the diffusion constant evaluated from the Einstein relation [Eq. (7)].

$$D = \frac{k_B T}{m} \tau_v \ , \tag{6}$$

where m is the molecular mass and k_B the Boltzmann constant. As a check of consistency, we have also evaluated D from the slope at long times of the mean-square displacement, using the Einstein relation

$$D = \lim_{t \to \infty} \frac{1}{6t} \langle |\mathbf{r}(t_0+t) - \mathbf{r}(t_0)|^2 \rangle \ . \tag{7}$$

In Table I we collect the values of the self-diffusion coefficient obtained from expressions (6) and (7). In general, we find that the values of the self-diffusion constant evaluated from (6) and (7) agree within 5%, which is within the estimated accuracy of the correlation times.

We have studied the temperature dependence of the self-diffusion coefficient in the isotropic phase. The simulation results for a fixed density ($\rho^* = 0.230$) and for temperatures in the range $0.45 < T^* < 2.00$ are shown in Fig. 4. The values of D^* as obtained from expressions (6) and (7) are summarized in Table II. Unlike the case of liquid argon [38] or low-anisotropy diatomic fluids [12], we could not reproduce the simulation results by using a linear relation between D^* and T^*. It seems that an exponential law of the form $D^* = D_0^* \exp(-A/T^*)$ with $D_0^* = 0.4086$ and $A = 0.6959$ fits the simulation results over the range of temperatures considered here.

Of particular interest is the behavior of the self-diffusion constant in the nematic phase. As the density is increased below the isotropic-nematic transition, D decreases as expected. For all the nematic state points, $D_\parallel > D_\perp$ (see Table I). This is also shown in Fig. 5. From this plot we can observe that, just above the transition, there is an enhancement in the parallel diffusion which results in an anomalous increase in $D_\parallel$ with density. While $D_\perp$ decreases monotonically as the system is compressed, $D_\parallel$ reaches a maximum at $\rho^* \approx 0.320$ and then decreases upon compression. This effect has been

TABLE II. Temperature-dependence of the self-diffusion coefficient in the isotropic phase at density $\rho^* = 0.230$.

T^*	D^*	D_E^*	$D_\parallel^*$	$D_\perp^*$	$D_\parallel^*/D_\perp^*$
0.45	0.096	0.097	0.105	0.092	1.15
0.50	0.095	0.097	0.100	0.093	1.07
0.55	0.112	0.118	0.124	0.105	1.17
0.60	0.129	0.125	0.160	0.114	1.40
0.65	0.148	0.147	0.157	0.144	1.09
0.70	0.138	0.145	0.147	0.133	1.10
0.75	0.158	0.163	0.185	0.144	1.28
0.80	0.178	0.187	0.188	0.174	1.08
0.85	0.185	0.190	0.212	0.171	1.24
0.90	0.188	0.198	0.201	0.182	1.10
0.95	0.202	0.211	0.259	0.174	1.49
1.00	0.207	0.211	0.209	0.206	1.02
1.05	0.199	0.217	0.224	0.187	1.20
1.10	0.195	0.205	0.223	0.182	1.23
1.15	0.212	0.214	0.250	0.193	1.29
1.25	0.250	0.249	0.267	0.241	1.11
1.50	0.252	0.261	0.269	0.243	1.10
2.00	0.320	0.336	0.341	0.310	1.10

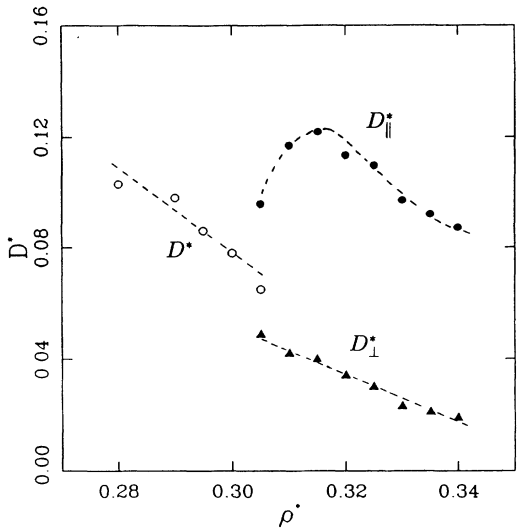

FIG. 5. Density effect on the self-diffusion coefficient in the isotropic-nematic region at $T^* = 0.95$. Open circles, isotropic phases; solid circles, parallel diffusion coefficient $D_\parallel^*$ in the nematic phase; triangles, perpendicular diffusion coefficient $D_\perp^*$ in the nematic phase.

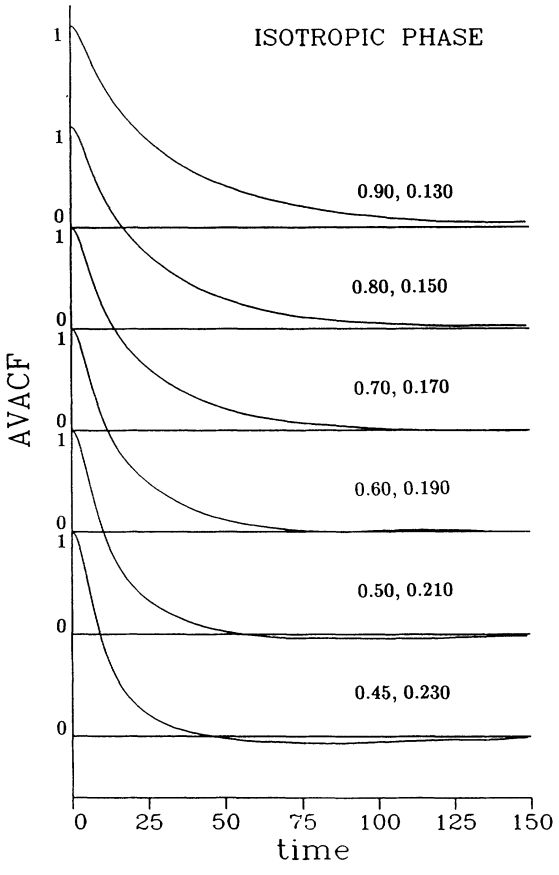

FIG. 6. Angular velocity autocorrelation function in the isotropic phase. The curves have been labeled according to the temperature and density in reduced units.

observed recently in the nematic phase of prolate and oblate hard ellipsoids of revolution [22], and has been ascribed to the particular density dependence of the nematic order parameter close to the transition.

What is also noticeable is that $D_{\parallel} > D_{\perp}$ even in the isotropic phase. Values of $D_{\parallel}/D_{\perp} > 1$ have been previously reported for molecular isotropic fluids [12, 14]. That this ratio does not actually equal 1 (as it should if the system is isotropic) is usually explained in terms of the fact that an upper time cutoff ($t_{\max}$) is used in the evaluation of the autocorrelation times. When $t_{\max} \to \infty$, the ratio $D_{\parallel}/D_{\perp}$ should tend to unity. There is a further effect, due to the finite size of the system, which makes $D_{\parallel}/D_{\perp}$ greater than unity. This can be seen by recalling that $D_{\parallel}/D_{\perp}$ can be expressed [39, 40] as

$$\frac{D_{\parallel}}{D_{\perp}} \approx \frac{(2\gamma+1)+2(1-\gamma)S}{(2\gamma+1)-(1-\gamma)S} , \tag{8}$$

where $\gamma = \pi/(4\kappa)$, and S is the order parameter. Due to the finite size of the system, S is not exactly zero in the isotropic phase, but takes values of the order $N^{-1/2}$, where N is the number of molecules. For the systems considered here ($N=256$, $\kappa=3$), values of $S \approx 0.10$ yield $D_{\parallel}/D_{\perp} \approx 1.15$.

Expression (8) can also be invoked to explain the rather high values of $D_{\parallel}/D_{\perp}$ on the isotropic side of the isotropic-nematic transition. In this region, the order parameter takes values appreciably higher than $N^{-1/2}$. According to (8), this results in $D_{\parallel}/D_{\perp} > 1$. In this case, the unusually high values of S below the transition, and not system-size effects, seem to be the main reason for the deviation from the ideal ratio. This enhancement in the parallel diffusion is a precursor effect of the proximity of an orientationally ordered phase.

IV. REORIENTATIONAL DYNAMICS

A. Reorientational motion

The molecular reorientational motion has been analyzed in terms of the angular velocity ACF (AVACF) and the torque ACF (TACF)

$$\phi_{\omega}(t) = \frac{\langle \boldsymbol{\omega}(t_0)\cdot\boldsymbol{\omega}(t_0+t)\rangle}{\langle \boldsymbol{\omega}(t_0)\cdot\boldsymbol{\omega}(t_0)\rangle} , \tag{9a}$$

$$\phi_{\Gamma}(t) = \frac{\langle \boldsymbol{\Gamma}(t_0)\cdot\boldsymbol{\Gamma}(t_0+t)\rangle}{\langle \boldsymbol{\Gamma}(t_0)\cdot\boldsymbol{\Gamma}(t_0)\rangle} , \tag{9b}$$

where $\boldsymbol{\omega}$ is the angular velocity perpendicular to the ma-

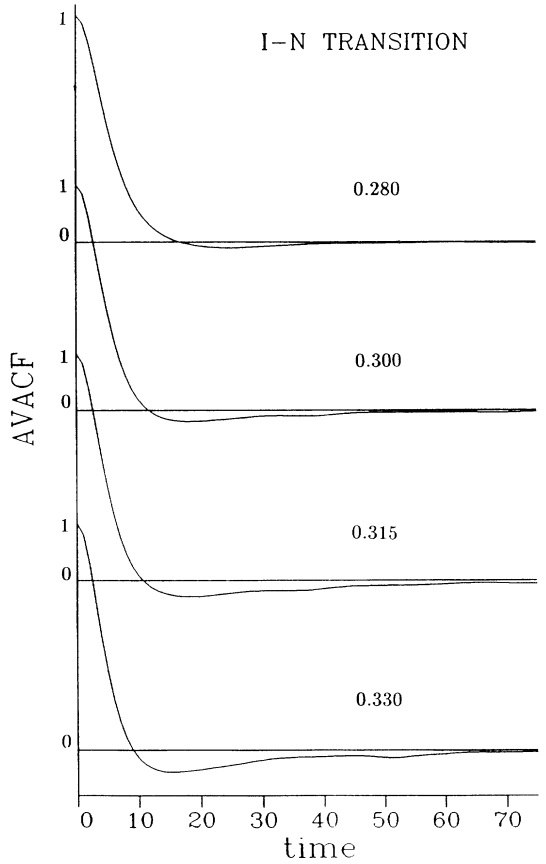

FIG. 7. Angular velocity autocorrelation function in the isotropic-nematic region at $T^*=0.95$. The curves have been labeled according to the density in reduced units.

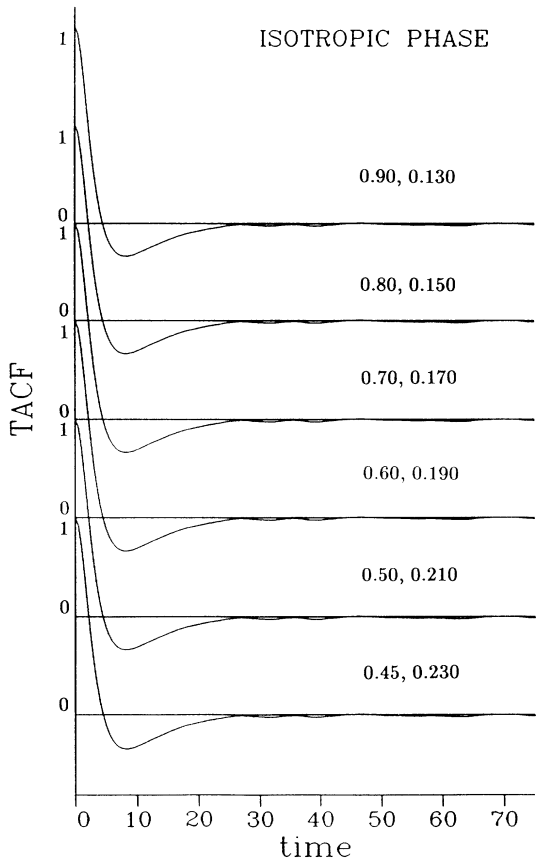

FIG. 8. Torque autocorrelation function in the isotropic phase. The curves have been labeled according to the temperature and density in reduced units.

jor symmetry axis of molecule i and Γ is the torque acting on each molecule. In addition, we have evaluated the reorientational ACF's ϕ_1 and ϕ_2, defined in (3).

The AVACF's in the isotropic phase are shown in Fig. 6. For the lower densities, these functions decay almost exponentially except at very short times. The decay becomes faster with increasing density or decreasing temperature and, for the highest density, the AVACF shows a negative minimum and a slow negative decay to zero. The AVACF's in the isotropic-nematic region are given in Fig. 7. They show the same qualitative features as those of typical dense molecular fluids [11–13,15]. As expected, the initial decay becomes faster and the negative region is more apparent with increasing density. The presence of negative regions is usually ascribed to a reversal in the direction of the angular momentum with respect to its initial value after a time lapse.

The TACF's are presented in Figs. 8 and 9. In all cases the initial decay is faster than that of the corresponding AVACF's. From the definition of ϕ_Γ, it follows that τ_Γ should be zero. For all state points, we found $\tau_\Gamma^* < 4\times 10^{-4}$, which is effectively zero when compared with the other correlation times.

Next we consider the reorientational ACF's. They are shown in Figs. 10 and 11 for the isotropic phase and the isotropic-nematic region, respectively. Due to the slow reorientational relaxation, especially at high densities, these ACF's were calculated covering a larger time span. In general, the long tail was calculated up to 1000–1200 t_0^*. For the lower densities, plots of the logarithms of ϕ_1 and ϕ_2 versus time show that, after an initial monotonic decay, they are oscillatory due to remnants of free-rotor behavior. Conversely, both functions decay almost exponentially at higher densities, $\phi_1(t)$ fitting more closely to an exponential than $\phi_2(t)$.

The relaxation times τ_l can be defined either from integration of the corresponding $\phi_l(t)$ following expression (3) ($\tau_{l,i}$), or from the slope at long times of the logarithmic plots of $\phi_l(t)$ versus time ($\tau_{l,s}$). Experimental information about the integral correlation time $\tau_{2,i}$ can be extracted from nuclear magnetic resonance measurements, while the slope correlation times can be related to the half-width of the Lorentzian far-infrared ($l=1$) and Raman ($l=2$) lines. If $\phi_l(t)$ were true exponentials, both correlation times $\tau_{l,i}$ and $\tau_{l,s}$ would be equal for all l values. However, this is not the case due to the non-Markovian nature of the reorientation process in its initial stage [41] (inertial regime). In Table III we have gathered the correlation times using both definitions. $\tau_{l,s}$

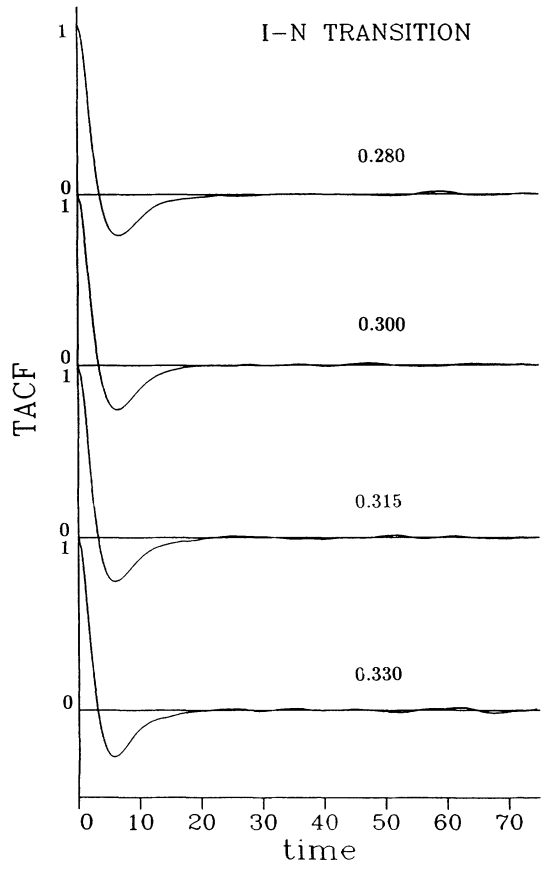

FIG. 9. Torque autocorrelation function in the isotropic-nematic region at $T^*=0.95$. The curves have been labeled according to the density in reduced units.

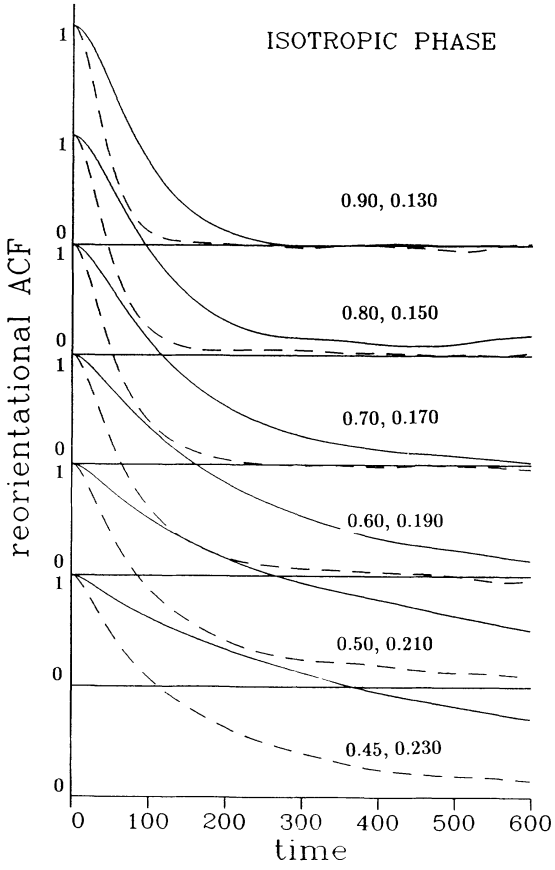

FIG. 10. Reorientational correlation functions $\phi_l(t)$ in the isotropic phase. Full line, $\phi_1(t)$; dashed line, $\phi_2(t)$. The curves have been labeled according to the temperature and density in reduced units.

TABLE III. Correlation times for the rotational motion of the GB fluid with $\kappa=3$ expressed in terms of the free rotation time $\tau^+=\tau(k_BT/I)^{1/2}$. The subscripts s and i stand for the slope correlation time and the integral correlation time of the reorientational correlation functions (see text).

T^*	ρ^*	τ_ω^+	$\tau_{1,s}^+$	$\tau_{2,s}^+$	$\tau_{1,i}^+$	$\tau_{2,i}^+$	$\tau_{1,i}^+/\tau_{2,i}^+$	$2\tau_{1,i}^+\tau_\omega^+$	$6\tau_{2,i}^+\tau_\omega^+$
					Isotropic phase				
0.45	0.230	0.09	4.89	1.94	4.98	1.85	2.68	0.91	1.01
0.50	0.210	0.12	4.34	1.69	4.30	1.52	2.83	1.05	1.11
0.60	0.190	0.20	2.35	0.79	2.60	1.04	2.50	1.06	1.27
0.70	0.170	0.26	1.51	0.55	1.83	0.82	2.22	0.97	1.30
0.80	0.150	0.35	1.08	0.43	1.65	0.79	2.08	1.16	1.68
0.90	0.130	0.48			1.31	0.65	2.03	1.25	1.85
					Isotropic nematic region				
0.95	0.280	0.072	6.38	2.37	6.61	2.42	2.73	0.96	1.05
0.95	0.290	0.054	8.32	3.05	8.52	3.13	2.72	0.92	1.01
0.95	0.295	0.057	8.08	3.16	8.29	3.22	2.58	0.94	1.10
0.95	0.300	0.039	10.33	3.79	10.48	3.83	2.74	0.82	0.90
0.95	0.305	0.034	11.44	4.47	11.58	4.37	2.65	0.79	0.90
0.95	0.310	0.018	16.60	6.18	16.69	6.17	2.70	0.60	0.67
0.95	0.315	0.014	19.74	7.04	19.80	7.04	2.81	0.54	0.58
0.95	0.320	0.014	20.43	7.62	20.50	7.63	2.69	0.56	0.62
0.95	0.325	0.008	27.74	9.35	27.78	9.36	2.97	0.44	0.45
0.95	0.330	0.009	28.27	9.72	28.31	9.74	2.90	0.49	0.51
0.95	0.335	0.005	36.02	12.19	36.05	12.46	2.89	0.37	0.39
0.95	0.340	0.006	37.30	12.72	37.32	12.74	2.93	0.43	0.44

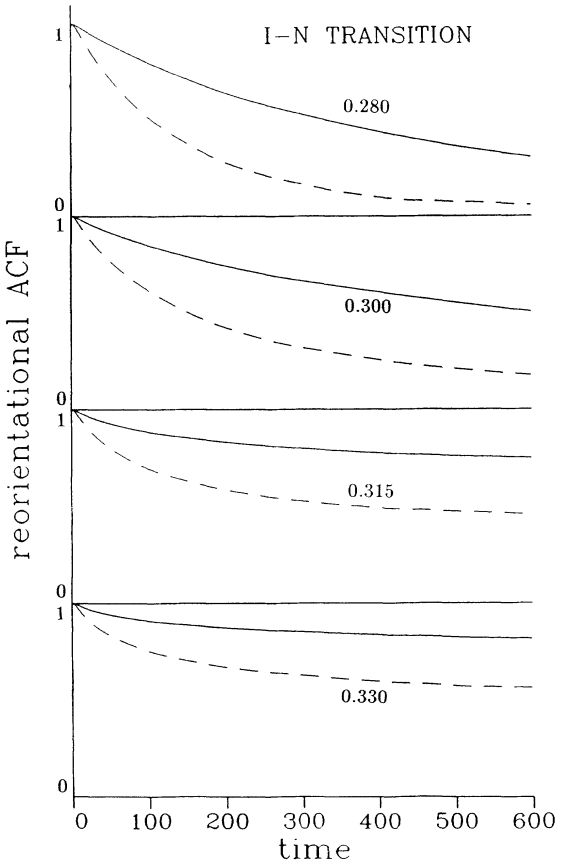

FIG. 11. Reorientational correction functions $\phi_l(t)$ in the isotropic-nematic region at $T^*=0.95$. Full line, $\phi_1(t)$; dashed line, $\phi_2(t)$. The curves have been labeled according to the density in reduced units.

was obtained from the gradient of $\ln\phi_l(t)$ versus time at long times, while $\tau_{l,i}$ was evaluated by integrating $\phi_l(t)$ numerically over the inertial regime and adding the contribution at larger times by assuming that the subsequent decay is exponential.

B. Reorientational models

In this section we compare the results obtained from our computer simulations with those from several theoretical models for molecular reorientation. Assuming a simple physical mechanism, these models predict different relations between the correlation times.

The simplest model is the classical Debye diffusion model (see, for instance, Ref. [3]), in which the reorientational process is a consequence of many small uncorrelated angular displacements. This results in

$$\ln\phi_l(t)=-l(l+1)D_Rt\ , \tag{10}$$

where D_R is the rotational diffusion constant. In this case, the orientational ACF's are exponentials *at all times* and the corresponding correlation times are linked through the relation

$$\frac{\tau_l}{\tau_{l+1}}=\frac{(l+2)}{l}\ . \tag{11}$$

In particular, the ratio τ_1/τ_2 should equal 3. From Table III, we can observe that τ_1/τ_2 is always less than 3, the departure from the Debye limit becoming more significant as the density is lowered or the temperature increased. Along the isotropic-nematic transition, this ratio is found to approach the Debye limit as the system is compressed. However, it should be noticed that this fact does not necessarily imply Debye-type (reorientation

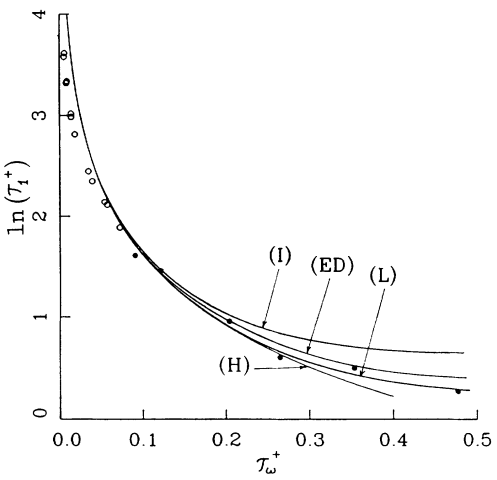

FIG. 12. Comparison of the simulation results for the correlation time $\tau_1^+(\tau_\omega^+)$ with predictions from models of molecular reorientation; (ED), Gordon's extended-diffusion model; (L), Langevin model; (I) Ivanov model; (H), Hubbard relationship. Open circles, simulation results for the isotropic-nematic region at $T^*=0.95$; solid circles, simulation results for the isotropic phase.

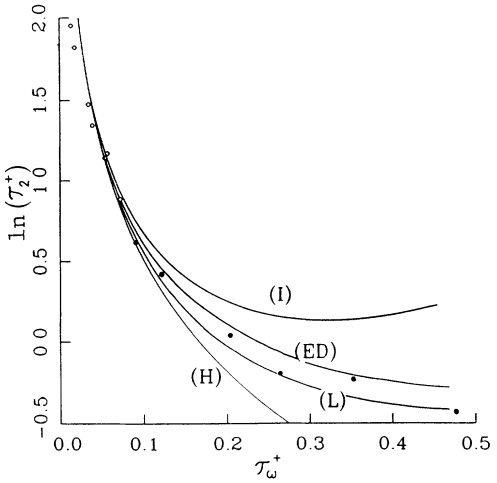

FIG. 13. Same as in Fig. 12, but for $\tau_2^+(\tau_\omega^+)$.

through small angles) orientational motion. For instance, Mansour, Murad, and Powles [17] have reported values of τ_1/τ_2 close to 3 at high temperatures and low densities in a computer simulation study of liquid ammonia. Under these conditions, at which molecules can rotate appreciably between successive collisions, it seems very unlikely that reorientation via small jumps would be the physical mechanism of reorientation.

We have also tested the validity of the Hubbard relation [42]

$$l(l+1)\tau_\omega^+\tau_l^+=1 \tag{12}$$

derived in terms of a diffusion model. In the above expression, the correlation times have been scaled by $(I/k_BT)^{1/2}$ (mean time for a classical free rotor in equilibrium at temperature T to rotate by an angle of order one radian), so that $\tau^+=\tau(k_BT/I)^{1/2}$. From Table III we see that this relation is approximately obeyed only at the higher densities in the isotropic phase. As the density is lowered, the left-hand side of (12) increasingly exceeds 1. It is also seen that the departure from unity is larger for $l=2$ than for $l=1$. Along the isotherm $T^*=0.95$, we observe that (12) is only approximately valid below the transition. As the system enters the nematic phase, the deviations from unity become significant. It should be noticed that, in contrast to the behavior found in the isotropic phase, in the nematic phase we find $l(l+1)\tau_\omega^+\tau_l^+<1$.

In Figs. 12 and 13 we show plots of τ_1^+ and τ_2^+ as functions of τ_ω^+ as predicted by the extended-diffusion model (ED), the Langevin model (L), and the Ivanov model (I) [43], along with the results obtained from our simulations. In the range of values of τ_ω^+ studied ($\tau_\omega^+<0.5$), these models yield rather similar values for $\tau_1^+(\tau_\omega^+)$. The differences in these models are more evident in the $\tau_2^+(\tau_\omega^+)$ plot. In general, we observe that in the isotropic phase, the results appear to be between the extended-diffusion model and the Langevin model. This should not be taken literally. These models predict that the mean lifetime of the correlations in the torque ACF should be negligibly small compared with τ_ω. Comparing ϕ_ω and ϕ_Γ we see that this condition is never met. In any case, the results show that the Ivanov model is not suitable for the GB fluid, at least under the conditions considered here.

As $\tau_\omega^+\to 0$, both models tend to the Hubbard relationship (12) (also included in Figs. 12 and 13). From the discussion above, we see that the limit of low τ_ω^+ is reached in the nematic liquid, for which (12), does not hold. We conclude that none of these models is able to explain the molecular reorientational mechanism in the nematic phase.

ACKNOWLEDGMENTS

This work has been supported by grants from NATO, DOE, and the Ministerio de Educación y Ciencia of Spain. Computer time for this work was kindly made available by the Centro Informático Científico de Andalucía (CICA) and the School of Chemical Engineering at Cornell University.

*Author to whom correspondence should be addressed.

[1] B. J. Berne and G. D. Harp, Adv. Chem. Phys. **17**, 63 (1970).

[2] D. J. Evans and G. P. Morris, *Nonequilibrium Statistical Mechanics* (Academic, New York, 1990).

[3] W. G. Rothschild, *Dynamics of Molecular Fluids* (Wiley, Interscience, New York, 1984).

[4] R. G. Gordon, J. Chem. Phys. **44**, 1830 (1966); see also D. Chandler, J. Chem. Phys. **60**, 3508 (1974).

[5] P. S. Hubbard, Phys. Rev. A **6**, 2421 (1972).

[6] E. Detyna, K. Singer, J. V. L. Singer, and A. J. Taylor, Mol. Phys. **41**, 31 (1980).
[7] A. G. St. Pierre and W. A. Steele, Mol. Phys. **43**, 123 (1981).
[8] W. A. Steele, Mol. Phys. **43**, 141 (1981).
[9] R. M. Lynden-Bell and I. R. McDonald, Mol. Phys. **43**, 1429 (1981).
[10] R. M. Lynden-Bell, in *Molecular Liquids: Dynamics and Interactions,* edited by A. J. Barnes *et al.* (Reidel, Dordrecht, 1984).
[11] P. S. Y. Cheung and J. G. Powles, Mol. Phys. **30**, 921 (1975); **32**, 1383 (1976).
[12] K. Singer, J. V. L. Singer, and A. J. Taylor, Mol. Phys. **37**, 1239 (1979).
[13] J. G. Powles, E. McGarth, and K. E. Gubbins, Mol. Phys. **40**, 179 (1980).
[14] O. Stenhauser and N. Neumann, Mol. Phys. **40**, 115 (1980).
[15] D. J. Tildesley and P. A. Madden, Mol. Phys. **48**, 129 (1983).
[16] R. M. Lynden-Bell, D. J. C. Hutchinson, and M. J. Doyle, Mol. Phys. **58**, 307 (1986).
[17] K. A. Mansour, S. Murad, and J. G. Powles, Mol. Phys. **65**, 785 (1988).
[18] R. M. Lynden-Bell, P. A. Madden, D. T. Stott, and R. J. Tough, Mol. Phys. **58**, 193 (1986).
[19] H. J. Böhm, C. Meissner, and R. Ahlrichs, Mol. Phys. **53**, 651 (1984).
[20] H. J. Böhm, R. M. Lynden-Bell, P. A. Madden, and I. R. McDonald, Mol. Phys. **51**, 761 (1984).
[21] D. W. Rebertus and K. M. Sando, J. Chem. Phys. **67**, 2585 (1977).
[22] M. P. Allen, Phys. Rev. Lett. **65**, 2881 (1990).
[23] M. P. Allen and D. Frenkel, Phys. Rev. Lett. **58**, 1748 (1987).
[24] J. Talbot, M. P. Allen, G. T. Evans, D. Frenkel, and D. Kivelson, Phys. Rev. A **39**, 4330 (1989).
[25] D. Frenkel and J. F. Maguirre, Mol. Phys. **49**, 503 (1983).
[26] J. J. Magda, H. T. Davis, and M. Tirrell, J. Chem. Phys. **85**, 6674 (1986).
[27] J. G. Gay and B. J. Berne, J. Chem. Phys. **74**, 3316 (1981).
[28] J. Kushick and B. J. Berne, J. Chem. Phys. **59**, 3732 (1973); **64**, 1362 (1976).
[29] D. Decoster, E. Constant, and M. Constant, Mol. Cryst. Liq. Cryst. **97**, 263 (1983).
[30] L. Tsykalo and A. D. Bagmet, Mol. Cryst. Liq. Cryst. **46**, 111 (1978).
[31] D. J. Adams, G. R. Luckhurst, and R. W. Phippen, Mol. Phys. **61**, 1575 (1987).
[32] G. R. Luckhurst, R. A. Stephens, and R. W. Phippen, Liq. Cryst. **8**, 451 (1990).
[33] E. de Miguel, L. F. Rull, M. K. Chalam, and K. E. Gubbins, Mol. Phys. **74**, 405 (1991).
[34] M. K. Chalam, K. E. Gubbins, E. de Miguel, and L. F. Rull, Mol. Simul. **7**, 357 (1991).
[35] E. de Miguel, L. F. Rull, M. K. Chalam, and K. E. Gubbins, Mol. Phys. **71**, 1223 (1990).
[36] E. de Miguel, L. F. Rull, M. K. Chalam, K. E. Gubbins, and F. van Swol, Mol. Phys. **72**, 593 (1991).
[37] R. Zwanzig and N. K. Ailawadi, Phys. Rev. **182**, 28 (1969).
[38] D. Levesque and L. Verlet, Phys. Rev. A **2**, 2514 (1970).
[39] K.-S. Chu and D. S. Moroi, J. Phys. (Paris) Colloq. **36**, C1-99 (1975).
[40] G. Vertogen and W. H. de Jeu, *Thermotropic Liquid Crystals, Fundamentals* (Springer, Heidelberg, 1988).
[41] P. A. Madden, in *Simulation of Properties of Spectroscopic Interest,* Proceedings of the International School of Physics "Enrico Fermi," Course XCVII, Varenna, 1985, edited by G. Ciccotti and W. G. Hoover (North-Holland, Amsterdam, 1986), p. 371.
[42] P. S. Hubbard, Phys. Rev. **131**, 1155 (1963).
[43] J. G. Powles and G. Rickayzen, Mol. Phys. **33**, 1207 (1977).